Measurements of Strong-Interaction Effects in Kaonic-Helium Isotopes at Sub-eV Precision with X-Ray Microcalorimeters

(J-PARC E62 Collaboration) Hashimoto, T.; Aikawa, S.; Akaishi, T.; Asano, H.; Bazzi, M.; Bennett, D. A.; Berger, M.; Bosnar, Damir; Butt, A. D.; Curceanu, C.; ...

Measurements of Strong-Interaction Effects in Kaonic-Helium Isotopes at Sub-eV Precision with X-Ray Microcalorimeters

T. Hashimoto,[1,2,*] S. Aikawa,[3] T. Akaishi,[4] H. Asano,[2] M. Bazzi,[5] D. A. Bennett,[6] M. Berger,[7] D. Bosnar,[8] A. D. Butt,[9] C. Curceanu,[5] W. B. Doriese,[6] M. S. Durkin,[6] Y. Ezoe,[10] J. W. Fowler,[6] H. Fujioka,[3] J. D. Gard,[6] C. Guaraldo,[5] F. P. Gustafsson,[7] C. Han,[2] R. Hayakawa,[10] R. S. Hayano,[11] T. Hayashi,[12] J. P. Hays-Wehle,[6] G. C. Hilton,[6] T. Hiraiwa,[13] M. Hiromoto,[4] Y. Ichinohe,[14] M. Iio,[15] Y. Iizawa,[3] M. Iliescu,[5] S. Ishimoto,[15] Y. Ishisaki,[10] K. Itahashi,[2] M. Iwasaki,[2] Y. Ma,[2] T. Murakami,[11] R. Nagatomi,[4] T. Nishi,[16] H. Noda,[17] H. Noumi,[13] K. Nunomura,[10] G. C. O'Neil,[6] T. Ohashi,[10] H. Ohnishi,[18] S. Okada,[19,2,†] H. Outa,[2] K. Piscicchia,[5] C. D. Reintsema,[6] Y. Sada,[18] F. Sakuma,[2] M. Sato,[15] D. R. Schmidt,[6] A. Scordo,[5] M. Sekimoto,[15] H. Shi,[7] K. Shirotori,[13] D. Sirghi,[5] F. Sirghi,[5] K. Suzuki,[7] D. S. Swetz,[6] A. Takamine,[2] K. Tanida,[1] H. Tatsuno,[10] C. Trippl,[7] J. Uhlig,[20] J. N. Ullom,[6] S. Yamada,[14] T. Yamaga,[2] T. Yamazaki,[11] and J. Zmeskal[7]

(J-PARC E62 Collaboration)

[1]Advanced Science Research Center, Japan Atomic Energy Agency (JAEA), Tokai 319-1184, Japan
[2]RIKEN Cluster for Pioneering Research, RIKEN, Wako 351-0198, Japan
[3]Department of Physics, Tokyo Institute of Technology, Tokyo 152-8551, Japan
[4]Department of Physics, Osaka University, Toyonaka 560-0043, Japan
[5]Laboratori Nazionali di Frascati dell' INFN, Frascati I-00044, Italy
[6]National Institute of Standards and Technology, Boulder, Colorado 80305, USA
[7]Stefan-Meyer-Institut für subatomare Physik, Vienna A-1030, Austria
[8]Department of Physics, Faculty of Science, University of Zagreb, Zagreb 10000, Croatia
[9]Politecnico di Milano, Dipartimento di Elettronica, Milano 20133, Italy
[10]Department of Physics, Tokyo Metropolitan University, Tokyo 192-0397, Japan
[11]Department of Physics, The University of Tokyo, Tokyo 113-0033, Japan
[12]Institute of Space and Astronautical Science, Japan Aerospace Exploration Agency, Sagamihara 252-5210, Japan
[13]Research Center for Nuclear Physics (RCNP), Osaka University, Ibaraki 567-0047, Japan
[14]Department of Physics, Rikkyo University, Tokyo 171-8501, Japan
[15]High Energy Accelerator Research Organization (KEK), Tsukuba 305-0801, Japan
[16]RIKEN Nishina Center for Accelerator-Based Science, RIKEN, Wako 351-0198, Japan
[17]Department of Earth and Space Science, Osaka University, Toyonaka 560-0043, Japan
[18]Research Center for Electron Photon Science (ELPH), Tohoku University, Sendai 982-0826, Japan
[19]Engineering Science Laboratory, Chubu University, Kasugai 487-8501, Japan
[20]Chemical Physics, Lund University, Lund 22100, Sweden

We have measured the $3d \to 2p$ transition x rays of kaonic ^{3}He and ^{4}He atoms using superconducting transition-edge-sensor microcalorimeters with an energy resolution better than 6 eV (FWHM). We determined the energies to be $6224.5 \pm 0.4(\text{stat}) \pm 0.2(\text{syst})$ eV and $6463.7 \pm 0.3(\text{stat}) \pm 0.1(\text{syst})$ eV, and widths to be $2.5 \pm 1.0(\text{stat}) \pm 0.4(\text{syst})$ eV and $1.0 \pm 0.6(\text{stat}) \pm 0.3(\text{stat})$ eV, for kaonic ^{3}He and ^{4}He, respectively. These values are nearly 10 times more precise than in previous measurements. Our results exclude the large strong-interaction shifts and widths that are suggested by a coupled-channel approach and agree with calculations based on optical-potential models.

The interaction and properties of mesons in nuclear matter are fundamental to hadron physics. Antikaons ($\bar{K}$) have been of great interest because their interaction with a nucleon (N) is known to be strongly attractive. The possible existence of kaonic nuclear bound states [1] and the role of $\bar{K}$ particles in high-density nuclear matter, such as neutron stars [2], have been widely discussed for decades.

Experimental study of these phenomena requires the $\bar{K}N$ interaction with low kinetic energy.

Two main experimental techniques have been used to study the $\bar{K}N$ interaction at low energies: $\bar{K}N$ free particle scattering and x-ray spectroscopy of kaonic atoms. For short-lived particles like kaons, x-ray spectroscopy provides a crucial anchor point near zero kinetic energy, while

scattering measurements are limited by the difficulty in making a low-energy kaon beam.

A kaonic atom is a Coulomb-bound system of a negatively charged antikaon (K^-) and an atomic nucleus. Spectroscopy of the x rays emitted as this system relaxes from its highly excited initial state probes the $\bar{K}N$ interaction. Constraints from kaonic hydrogen experiments are essential to establish the attractive nature of the $\bar{K}N$ interaction in the isospin 0 channel [3,4]. Heavier atoms provide information on the $\bar{K}N$ interaction in the nuclear medium, and support an attractive $\bar{K}$ nucleus potential; however, the strength of the attraction remains uncertain [5,6]. More accurate x-ray measurements will allow quantitative evaluations of the potential.

Kaonic helium isotopes are of special interest in connection to the light kaonic nuclear states, such as the $\bar{K}NN$ state reported by J-PARC E15 [7,8] and other pioneering works [9–11]. This state is naively supposed to be an s-wave state, while the atomic $2p$ state in kaonic helium, which is the most tightly bound atomic state that has been observed with x rays so far, is sensitive to the existence of p-wave nuclear bound states. Theoretical calculations based on typical optical potential models predict a small shift (<1 eV) from the Coulomb value and a small additional absorption width (~2 eV) due to the strong interaction [12]. On the other hand, calculations involving a coupled-channel potential allow large shifts (>1 eV) and widths (>5 eV) if the potential is deep enough to accommodate a p-wave nuclear state [13].

Energy resolution on the electron-volt scale is necessary to experimentally resolve the discrepancy described above. Recent measurements of kaonic helium atoms made by KEK-E570 [14] and SIDDHARTA [15,16] used silicon drift detectors, whose resolution is limited to 150 eV FWHM at 6 keV. Subelectron-volt energy resolution has been achieved by wavelength-dispersive crystal spectrometers in pionic-atom experiments [17]. However, their low collection efficiency, typically $O(10^{-7})$, is not practical for kaonic-atom experiments because of limited K^- beam intensity and, consequently, very low x-ray flux. There is only one published experiment that used a diffraction-based spectrometer to observe kaonic atoms [18], and the resolution achieved was not as good as in the pionic-atom case [19].

Our new approach is to use a superconducting transition-edge sensor (TES) microcalorimeter spectrometer. A TES pixel utilizes the steep temperature dependence of the electrical resistance at the superconducting phase transition to measure the thermal energy generated by an x-ray photon with an excellent energy resolution [20]. A large collecting area can be obtained with an array of these sensors [21]. In this Letter, we report the first measurement of kaonic-atom x rays with a TES spectrometer. We measured x rays from the $3d \rightarrow 2p$ transitions in kaonic ^{3}He and ^{4}He atoms and extracted the $2p$ shifts and widths with subelectron volt precisions.

The experiment (J-PARC E62) was carried out at the K1.8BR beam line of the J-PARC hadron experimental facility [22], in June 2018. Total data acquisition times were 198 and 149 h for the ^{3}He and ^{4}He targets, respectively, at a primary proton beam intensity of 51 kW. Negatively charged kaons emerging from the beam line at 900 MeV/c were stopped in a liquid-helium target after passing through copper degrader blocks. The typical number of the K^- beam particles without the degraders was 1.1×10^5 per pulse. Pulses were 2 s in length and the on-off-repetition cycle period was 5.2 s. The beam contained approximately 5 pions per K^-. The kaon stopping efficiencies in the 400 mL liquid target at 1.4 K are estimated to be 0.06% and 0.08% for ^{3}He and ^{4}He, respectively.

The TES x-ray spectrometer [21] was of the same type as used in the pionic-atom experiment at the Paul Scherrer Institute [23] and the same spectrometer unit later used in muonic atom experiments at J-PARC MLF [24,25] and XAFS measurements at SPring-8 [26]. Each TES in the 240-pixel array consists of a bilayer of thin molybdenum and copper films. A 4 μm-thick bismuth absorber on each sensor leads to an 85% quantum efficiency at 6 keV. The effective area of each pixel, defined by an aperture just above the array, is 305×290 μm. Thus, the total active area of the array is approximately 21 mm^2. The TES detector was installed in the same vacuum with the cryostat of the target, 75 mm away from the beam axis, and 10 mm behind a 300 μm-thick beryllium x-ray window of the target cell [27]. The total collection efficiency of the TES array for all 6 keV x rays emitted into 4π sr from the target volume was 2.4×10^{-4}.

The TES spectrometer was cooled by a pulse-tube-backed adiabatic demagnetization refrigerator and the bath temperature was regulated at 70 mK. Because the pulsed dc beam structure at J-PARC disturbs the spectrometer's temperature regulation, we tuned the kaon beam and installed lead shielding blocks to reduce the flux of charged beam particles, which are mainly contaminating pions, on the TES system. As a result, the temperature fluctuation in the thermal bath of the spectrometer was as good as $6 - 8$ μK rms. Without the kaon beam, the typical rms fluctuation was 5 μK [28].

The TES-current signals were read out via the time division multiplexing technique at a sampling interval of 7.2 μs [29]. The time scale of the (thermal) detector response is on the order of milliseconds. Data records for each TES pixel were 1024 samples (7.4 ms) long and were edge triggered to capture a "pulse" in the TES current. Each pulse record is analyzed to extract a single estimator of pulse height via linear optimal filtering and a standard analysis procedure [30,31].

To mitigate the effects of the charged-particle beam line environment, several analysis techniques are employed. The on-off cycling of the kaon beam creates gain structures in the TES spectrometer, which are corrected based on the

x-ray-event timing within the kaon-beam cycle [28]. Charged particles striking the silicon frame of the TES array deposit enough energy to cause significant temperature shifts in nearby pixels, which appear as bumps in the measured TES pulse. To reduce the time window in which these small cross talk pulses can affect the signal pulse, only 324 samples out of the full 1024 recorded samples are used to reconstruct the pulse-height estimator [32]. Charged particles passing through a TES detector can be misidentified as several kiloelectron volt energy events. However, most charged particles that pass through a TES pixel will also transfer energy to adjacent pixels, so multipixel analysis is employed to identify and cut these charged-particle-induced pulses [33].

After all the analysis optimizations, and at a cost of 32%–35% event loss, the energy resolution with the kaon beam on is 5.5–5.7 eV FWHM, measured at the Co $K\alpha$ line (6.93 keV). Without our optimizations, the energy resolution is about 8 eV with the beam on. Without the kaon beam, the inherent energy resolution is 5.1–5.3 eV. Our targeted data cuts to remove charged-particle events also give a more Gaussian-like response in the spectrometer. Importantly, the exponential, high-energy-tail structure observed in our pionic-atom experiment [23,34] is negligibly small in the spectroscopic data presented here.

The TES spectrometer was energy calibrated for each pixel via a ladder of K x-ray lines from high-purity metals of chromium, cobalt, and copper. These calibration lines are excited by a commercial x-ray tube source and are observed concurrently with the kaonic-atom x-ray signal. Each characteristic x-ray line in the pulse-height histogram is fitted to line profiles from the literature [35]. Then, we construct temporal calibration curves using measured pulse heights (P) and the known energies (E) [35]. The calibration curve is a form of $E = P/g(P)$, where the gain g is a cubic spline [31]. The x-ray data are broken into observation periods of 4–8 h: for each pixel, the calibration curve is recalculated for each new period.

In addition to the six intense calibration lines, we observe the Fe $K\alpha$ line due to the emission from various stainless-steel parts. We can use a spectrum coadded across all pixels to track the Fe $K\alpha$ line shift vs time and separately use a spectrum coadded across all datasets to observe pixel-specific shifts. Then, we created the final calibration curves with the Fe $K\alpha$ position calculated including these two shifts. Figure 1 shows the x-ray spectrum using these final calibration curves.

In fitting the experimental spectrum to the line profiles, the detector energy-response function is taken to be a Bortels function [36], the convolution of a Gaussian with the normalized sum of a one-sided exponential tail to the low-energy side and a delta function. The tail results from incomplete thermalization of the x-ray energy in the evaporated-bismuth absorber of each TES [37,38]. This function has three parameters: the Gaussian energy
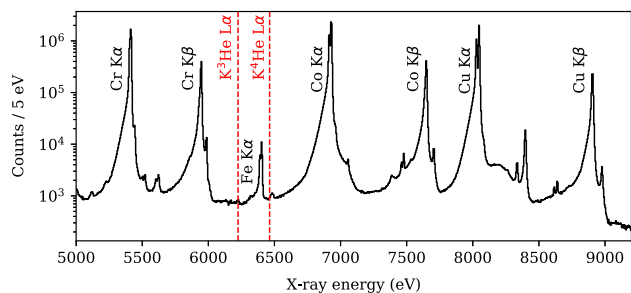

FIG. 1. TES-measured x-ray spectrum summed across all the ^{3}He data. The characteristic lines used for the energy calibration are labeled. The expected $3d \to 2p$ x-ray energies from the kaonic ^{3}He and ^{4}He are indicated as dotted lines. The small feature near 6500 eV, just above the K^{-4}He $L\alpha$ energy, is the Bi $M\beta$ escape peak of the Cu $K\beta$ line.

resolution (δE) and the scale length (λ) and the fraction (f_{tail}) of the low-energy tail. δE and f_{tail} increase linearly with energy, while λ is nearly constant over energy [34]. f_{tail} and λ are found to be uniform among the pixels and across time, thus, we fix these parameters at common values that are obtained from the fitting to the summed spectrum of the full dataset.

The accuracy of the calibration curves is assessed by cross-validation tests similar to that made by Fowler *et al.* [31], in which new calibration curves are constructed with one anchor point deliberately omitted. By comparing the known energy of the omitted point with the energy of this point predicted by the new curve, the fidelity of the curve at each anchor point is tested. Our tests indicate that the absolute energy has a 0.08 eV uncertainty for a 100-eV distance to the nearest anchors. In addition, we allow a 0.07 eV systematic error for possible undetected features in the spectra and the systematic uncertainty of the calibration energies [31].

Figure 2(a) shows the correlation between the energy deposited in the last beam counter in front of the target and the timing of the TES pulses with respect to the kaon beam. Most of the minimum ionizing particles (MIP), which come
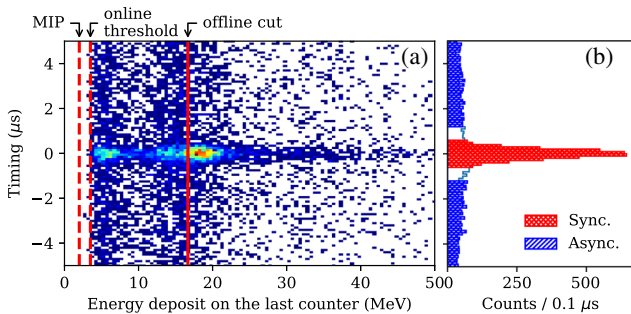

FIG. 2. (a) Correlation between the energy deposited (dE) in the last beam counter and the TES pulse timing. (b) Timing histogram of the TES pulses with $dE > 16$ MeV. The hatches show the timing ranges of kaonic-atom formation events and asynchronous-background events. These plots include events in the x-ray energy range of $6100 < E < 6600$ eV.
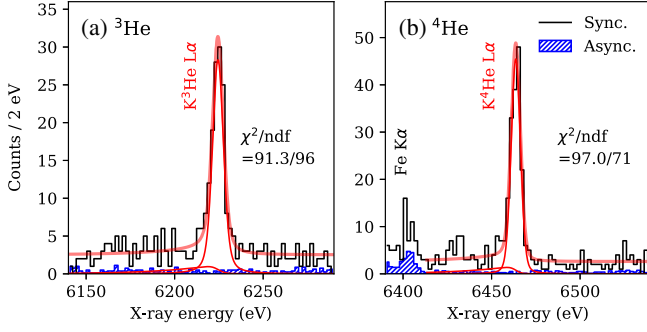
FIG. 3. Final x-ray spectra after all event selections. The asynchronous background was estimated via the timing ranges defined in Fig. 2. The peak fitting lines, including decomposition into the main peak and the low-energy tail components, are shown.

from kaon decays and reactions, were removed by the online hardware threshold. Additionally, we required the energy deposit to be larger than 16 MeV to select low momentum kaons which are likely to stop in the target. This off-line selection further reduces the background by half. Figure 2(b) shows the projection to the timing axis and the definitions of timing ranges synchronous and asynchronous to the kaon beam, where a clear peak is observed with a 500 ns FWHM resolution.

The final x-ray spectra obtained with the timing range synchronous to the kaon beam are shown in Fig. 3. The $3d \rightarrow 2p$ x-ray lines from kaonic helium isotopes are clearly observed. The asynchronous background contributions, shown with a normalization by the time-range width, are negligibly small. The dominant contribution to the background is attributed to the kaon beam itself or to secondary particles from the kaon-absorption reactions around the target. The pulse time-range selection slightly changes the peak energies and the energy resolutions. This effect is quantified as part of the systematic uncertainties.

The kaonic x-ray peaks are fitted in the TES spectra to extract the intrinsic peak energies and widths. We employ a single Lorentzian function for each intrinsic line shape. This is justified because there is no fine splitting for a spin-0 K^- meson, and parallel transitions have a vanishingly small probability due to the large K^- absorption width. The detector response, namely δE, f_{tail}, and λ at the kaonic x-ray energies, are estimated separately via the calibration lines. The energies ($E_{3d \rightarrow 2p}$) and widths (Γ_{2p}) of the x-ray lines of kaonic helium isotopes are obtained to be

$$E_{3d \rightarrow 2p}^{K^{-3}\text{He}} = 6224.5 \pm 0.4(\text{stat}) \pm 0.2(\text{syst}) \text{ eV},$$

$$E_{3d \rightarrow 2p}^{K^{-4}\text{He}} = 6463.7 \pm 0.3(\text{stat}) \pm 0.1(\text{syst}) \text{ eV},$$

$$\Gamma_{2p}^{K^{-3}\text{He}} = 2.5 \pm 1.0(\text{stat}) \pm 0.4(\text{syst}) \text{ eV},$$

$$\Gamma_{2p}^{K^{-4}\text{He}} = 1.0 \pm 0.6(\text{stat}) \pm 0.3(\text{syst}) \text{ eV}.$$

Systematic uncertainties are classified into the following four sources, and the estimated results are summarized in

TABLE I. Measured x-ray energies and widths of the kaonic ^{3}He and ^{4}He $3d \rightarrow 2p$ transitions, together with the summary of the statistical and systematic errors. Electromagnetic calculated energies are also tabulated. All the values are in units of eV.

	K^{-3}He		K^{-4}He	
	Energy	Width	Energy	Width
Measured ($E_{3d \rightarrow 2p}^{\text{exp}}$, Γ_{2p})	6224.48	2.5	6463.69	1.0
Statistical error	0.40	1.0	0.27	0.6
Systematical error: total	0.18	0.4	0.11	0.3
(a) Absolute energy scale	0.17	$\cdots$	0.09	$\cdots$
(b) Detector resolution	0.01	0.2	0.01	0.1
(c) Low-energy tail	0.03	0.1	0.03	0.1
(d) Fitting robustness	0.05	0.3	0.05	0.3
Electromagnetic ($E_{3d \rightarrow 2p}^{\text{e.m.}}$)	6224.69	$\cdots$	6463.46	$\cdots$
Error from the K^- mass	0.17	$\cdots$	0.18	$\cdots$
$\Delta E_{2p} \equiv E_{3d \rightarrow 2p}^{\text{exp}} - E_{3d \rightarrow 2p}^{\text{e.m.}}$	-0.21	$\cdots$	0.23	$\cdots$

Table I. (a) The calibration accuracy is the main systematic error and is energy dependent as already discussed above. (b) The uncertainty of the energy resolution of the detector comes from the pulse time-range selection and the addition of spectra from pixels whose energy-calibration curves differ from one another. The latter broadening term is evaluated by the cross-validation tests. (c) The uncertainties in the tail parameters (f_{tail}, λ) are evaluated by the cross-validation tests and the distribution of the parameters obtained by fitting the tail parameters separately for each pixel. (d) Robustness of the fitting process is tested against the changes to the fit regions, different binning of the histogram, and the choice of background model (constant or linear slope).

The strong-interaction shifts are extracted from the measured kaonic energies ($E_{3d \rightarrow 2p}^{\text{exp}}$) and the electromagnetic energies calculated without the strong interaction ($E_{3d \rightarrow 2p}^{\text{e.m.}}$). The electromagnetic energy of each orbital is calculated by considering vacuum polarization to the next-to-leading order and the relativistic recoil effect [39]. The uncertainty on the charged kaon mass, tabulated by the particle data group as 493.677(16) MeV/c^2 [40], translates to a non-negligible absolute uncertainty of $\sim$0.2 eV for the calculated x-ray energies. The precision of the calculation itself is better than 0.01 eV including the uncertainty of the electron screening effect [39]. Then, the strong interaction shifts in the $2p$ states of kaonic helium isotopes ($\Delta E_{2p} \equiv E_{3d \rightarrow 2p}^{\text{exp}} - E_{3d \rightarrow 2p}^{\text{e.m.}}$) are

$$\Delta E_{2p}^{K^{-3}\text{He}} = -0.2 \pm 0.4(\text{stat}) \pm 0.3(\text{syst}) \text{ eV},$$

$$\Delta E_{2p}^{K^{-4}\text{He}} = 0.2 \pm 0.3(\text{stat}) \pm 0.2(\text{syst}) \text{ eV}.$$

The difference between the $2p$ shifts in kaonic helium isotopes ($\Delta E_{2p}^{\text{isotope}} \equiv \Delta E_{2p}^{K^{-3}\text{He}} - \Delta E_{2p}^{K^{-4}\text{He}}$) is
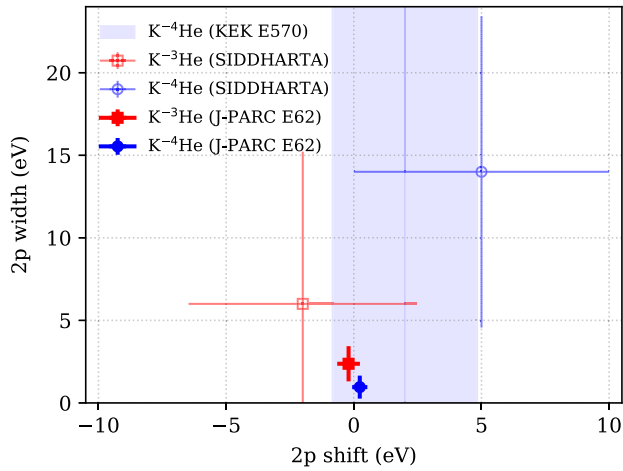
FIG. 4. Strong-interaction shifts and widths in the $2p$ state of kaonic-helium atoms. Results in this Letter (J-PARC E62) are compared to the past measurements of the SIDDHARTA [16] and the KEK E570 experiments [14]. The KEK E570 result is shown as a band because no width value is reported. The errors quoted here are the quadratic sum of the statistical and systematical errors. The uncertainty in the electromagnetic calculation is not considered.

$$\Delta E_{2p}^{\text{isotope}} = -0.4 \pm 0.5(\text{stat}) \pm 0.2(\text{syst}) \text{ eV}.$$

Here, the uncertainty that originates from the charged-kaon mass is almost canceled, making this result useful for future comparisons to theoretical calculations.

The shifts and widths determined in this Letter are compared to those of the past experiments in Fig. 4. Our results improve the precisions by about a factor of 10, and clearly exclude the large shift $|\Delta E_{2p}| > 1$ eV and a large width $\Gamma_{2p} > 5$ eV. The optical-potential-model approach works rather well in these light systems.

This is the first experiment in which a finite width of a few electron volts is directly determined for an atomic state of kaonic atoms, whereas all the past reported widths below 10 eV are indirect measurements based on x-ray yields [5]. In turn, from the $2p$ width of this Letter and the x-ray yields of all the transitions to the $2p$ states in the literature [41], we can estimate the $K\alpha$ yields of kaonic helium to be of the order of 0.01% per stopped kaon. This suggests the possibility of a future experiment to measure $1s$ states with large-collecting-area devices, such as silicon drift detectors.

In summary, we measured the energies and widths of the $3d \to 2p$ transition x rays from kaonic ^{3}He and ^{4}He atoms with a TES microcalorimeter spectrometer. With an energy resolution better than 6 eV (FWHM), we achieved approximately 10 times better precision than in the past experiments. Our results exclude the large shifts and widths predicted by a coupled-channel calculation and are compatible with the optical-model-based calculations. Comparison to more elaborate theoretical studies would

be beneficial for the precise evaluation of the $\bar{K}$-nucleus strong interaction, especially in connection to the properties of light kaonic nuclei. The present experiment demonstrates that TES detectors can perform physics experiments such as measuring a rare signal of one event per hour even in a difficult beam environment that produces many charged particles. This marks an important milestone for the widespread use of high-resolution microcalorimeter spectrometers in harsh radiation environments, while the range of applications is expanding rapidly by covering a higher energy range and a larger effective area.

*tadashi.hashimoto@a.riken.jp
†sokada@isc.chubu.ac.jp

[1] Y. Akaishi and T. Yamazaki, Phys. Rev. C **65**, 044005 (2002).
[2] D. B. Kaplan and A. E. Nelson, Phys. Lett. B **175**, 57 (1986).
[3] M. Iwasaki et al., Phys. Rev. Lett. **78**, 3067 (1997).
[4] M. Bazzi et al., Phys. Lett. B **704**, 113 (2011).
[5] C. J. Batty, E. Friedman, and A. Gal, Phys. Rep. **287**, 385 (1997).
[6] S. Hirenzaki, Y. Okumura, H. Toki, E. Oset, and A. Ramos, Phys. Rev. C **61**, 055205 (2000).
[7] S. Ajimura et al., Phys. Lett. B **789**, 620 (2019).
[8] T. Yamaga et al., Phys. Rev. C **102**, 044002 (2020).
[9] FINUDA Collaboration, Phys. Rev. Lett. **94**, 212303 (2005).
[10] T. Yamazaki et al., Phys. Rev. Lett. **104**, 132502 (2010).
[11] Y. Ichikawa et al., Prog. Theor. Exp. Phys. **2015**, 021D01 (2015).
[12] E. Friedman, Hyperfine Interact. **209**, 127 (2012).
[13] Y. Akaishi, Proceedings of EXA2005 (2006), 10.1553/exa05s45.

[14] S. Okada *et al.*, Phys. Lett. B **653**, 387 (2007).

[15] SIDDHARTA Collaboration, Phys. Lett. B **697**, 199 (2011).

[16] M. Bazzi *et al.*, Phys. Lett. B **714**, 40 (2012).

[17] D. Gotta, Prog. Part. Nucl. Phys. **52**, 133 (2004).

[18] A. S. Denisov *et al.*, JETP Lett. **54**, 558 (1991), http://jetpletters.ru/ps/1266/article_19151.shtml.

[19] M. Trassinelli *et al.*, Phys. Lett. B **759**, 583 (2016).

[20] K. D. Irwin and G. C. Hilton, in *Cryogenic Particle Detection*, edited by C. Enss (Springer, Berlin, 2005), pp. 63–150.

[21] W. B. Doriese *et al.*, Rev. Sci. Instrum. **88**, 053108 (2017).

[22] K. Agari *et al.*, Prog. Theor. Exp. Phys. **2012**, 02B009 (2012).

[23] S. Okada *et al.*, Prog. Theor. Exp. Phys. **2016**, 091D01 (2016).

[24] S. Okada *et al.*, J. Low Temp. Phys. **200**, 445 (2020).

[25] T. Okumura *et al.*, Phys. Rev. Lett. **127**, 053001 (2021).

[26] S. Yamada *et al.*, Rev. Sci. Instrum. **92**, 013103 (2021).

[27] T. Hashimoto *et al.*, J. Low Temp. Phys. **199**, 1018 (2020).

[28] T. Hashimoto *et al.*, IEEE Trans. Appl. Supercond. **27**, 1 (2017).

[29] W. B. Doriese *et al.*, J. Low Temp. Phys. **184**, 389 (2016).

[30] J. W. Fowler, B. K. Alpert, W. B. Doriese, Y.-I. Joe, G. C. O'Neil, J. N. Ullom, and D. S. Swetz, J. Low Temp. Phys. **184**, 374 (2016).

[31] J. W. Fowler *et al.*, Metrologia **58**, 015016 (2021).

[32] H. Tatsuno *et al.*, J. Low Temp. Phys. **200**, 247 (2020).

[33] R. Hayakawa *et al.*, J. Low Temp. Phys. **200**, 269 (2020).

[34] H. Tatsuno *et al.*, J. Low Temp. Phys. **184**, 930 (2016).

[35] G. Hölzer, M. Fritsch, M. Deutsch, J. Härtwig, and E. Förster, Phys. Rev. A **56**, 4554 (1997).

[36] G. Bortels and P. Collaers, Int. J. Rad. Appl. Instrum. A **38**, 831 (1987).

[37] D. Yan *et al.*, Appl. Phys. Lett. **111**, 192602 (2017).

[38] G. C. O'Neil *et al.*, J. Low Temp. Phys. **199**, 1046 (2020).

[39] J. P. Santos, F. Parente, S. Boucard, P. Indelicato, and J. P. Desclaux, Phys. Rev. A **71**, 032501 (2005).

[40] Particle Data Group, Prog. Theor. Exp. Phys. **2020**, 083C01 (2020).

[41] M. Bazzi *et al.*, Eur. Phys. J. A **50**, 91 (2014).